NEOPLASIA
www.neoplasia.com

Volume 20 Number 6 June 2018 pp. 621–631 621

Aging Increases Susceptibility to Ovarian Cancer Metastasis in Murine Allograft Models and Alters Immune Composition of Peritoneal Adipose Tissue[1]

Elizabeth A. Loughran[*,†,‡], Annemarie K. Leonard[*,‡], Tyvette S. Hilliard[*,‡], Ryan C. Phan[‡], Madeleine G. Yemc[‡], Elizabeth Harper[*,‡], Emma Sheedy[‡], Yuliya Klymenko[‡,§], Marwa Asem[*,†,‡], Yueying Liu[*,‡], Jing Yang[*,‡], Jeff Johnson[*,‡], Laura Tarwater , Zonggao Shi[*,‡], Matthew Leevy[‡,§], Matthew J. Ravosa[‡,§,¶,#] and M. Sharon Stack[*,‡]

[*]Department of Chemistry and Biochemistry, University of Notre Dame, Notre Dame, IN; [†]Integrated Biomedical Sciences Graduate Program, University of Notre Dame, Notre Dame, IN; [‡]Harper Cancer Research Institute, University of Notre Dame, Notre Dame, IN; [§]Department of Biological Sciences, University of Notre Dame, Notre Dame, IN; [¶]Department of Aerospace and Mechanical Engineering, University of Notre Dame, Notre Dame, IN; [#]Department of Anthropology, University of Notre Dame, Notre Dame, IN

Abstract

Ovarian cancer, the most deadly gynecological malignancy in U.S. women, metastasizes uniquely, spreading through the peritoneal cavity and often generating widespread metastatic sites before diagnosis. The vast majority of ovarian cancer cases occur in women over 40 and the median age at diagnosis is 63. Additionally, elderly women receive poorer prognoses when diagnosed with ovarian cancer. Despite age being a significant risk factor for the development of this cancer, there are little published data which address the impact of aging on ovarian cancer metastasis. Here we report that the aged host is more susceptible to metastatic success using two murine syngeneic allograft models of ovarian cancer metastasis. This age-related increase in metastatic tumor burden corresponds with an increase in tumor infiltrating lymphocytes (TILs) in tumor-bearing mice and alteration of B cell-related pathways in gonadal adipose tissue. Based on this work, further studies elucidating the status of B cell TILs in mouse models of metastasis and human tumors in the context of aging are warranted.

Neoplasia (2018) 20, 621–631

Introduction

Ovarian cancer (OvCa) is the leading cause of death due to gynecological malignancy in women in the United States. Often diagnosed with metastases, patients with ovarian cancer receive poor prognoses [1]. The vast majority of OvCas are epithelial in origin with predominantly serous (70%–85%) and endometrioid (10%) histotypes [2,3]. OvCa metastasizes uniquely when tumor cells or multicellular aggregates detach from the primary tumor and disseminate throughout the peritoneal cavity, forming metastatic sites on the peritoneum [1]. Additionally, hematogenous metastasis with metastatic homing to the ovary has been seen in model systems [4,5].

Aging is a significant risk factor and prognostic factor for women with OvCa, wherein the median age at diagnosis is 63 [6]. Furthermore, elderly patients have poorer prognoses, with unfavorable progression-free survival (PFS) and overall survival associated with increased age [7–11]. While treatment disparities in the elderly

Address all Correspondence to: M. Sharon Stack, University of Notre Dame, Harper Cancer Research Institute, 1234 Notre Dame Ave., A200 Harper Hall South Bend, IN 46617.
E-mail: sstack@nd.edu
[1] The authors have no conflicts of interest to disclose.
Received 5 February 2018; Revised 20 March 2018; Accepted 26 March 2018

© 2018 . Published by Elsevier Inc. on behalf of Neoplasia Press, Inc. This is an open access article under the CC BY-NC-ND license (http://creativecommons.org/licenses/by-nc-nd/4.0/).
1476-5586/18
https://doi.org/10.1016/j.neo.2018.03.007

may contribute to this difference, the aged host may also be more susceptible to disease progression. There is a paucity of studies addressing the impact of aging on OvCa metastasis.

The fact that OvCa is so often diagnosed at metastatic stages of the disease confounds the ability of researchers to draw conclusions about the relationship between metastasis and age from patient data. Thus, to evaluate this relationship, research models of metastasis are required. *In vitro* models using human omental mesothelial cells (HOMCs) have demonstrated that HOMCs from elderly patients are in a pro-inflammatory state [12]. Another study showed an increase in adhesion of OvCa cells to HOMCs in a state of induced senescence *in vitro* [13]. While a single ovarian cancer metastasis study has utilized middle-aged mice [14], studies designed to evaluate the impact of age on metastasis *in vivo* have not been reported.

The purpose of this study was to test the hypothesis that age impacts the metastatic outcome of OvCa. Here we utilize distinct syngeneic murine models of OvCa metastasis to demonstrate that age increases the susceptibility of the host to metastasis. Our data suggest that the immune composition of aged peritoneal adipose tissue, specifically B cells, may contribute to this age-related disparity in metastasis.

Materials and Methods

Murine Aging Models

Two age groups of C57Bl/6 female mice (Jackson Laboratories) were used for this study. Retired breeders were purchased around 8 months of age and allowed to age until they reached 20 months, at which point they are devoid of ovarian follicles [15]. Young mice were bred once beginning at 8 weeks and were used between 4–6 months of age. Mouse age time points were chosen based on research on mouse-human lifespan equivalencies [16]. In this murine model of aging, mice 3–6 months (young) and 20–23 months (aged) correspond to humans 20–30 and 60–67 years of age, respectively (Figure 1A). The same methods were used for experiments with FVB/NJ mice (Jackson Laboratories), which have a comparable lifespan to C57Bl/6 mice [17]. All animal procedures were carried out according to the regulations of the Institutional Animal Care and Use Committee at The University of Notre Dame.

Murine Allograft Models

Two allograft models were utilized in this study. Parental ID8 cells, a C57Bl/6 syngeneic mouse ovarian surface epithelial (MOSE) cell

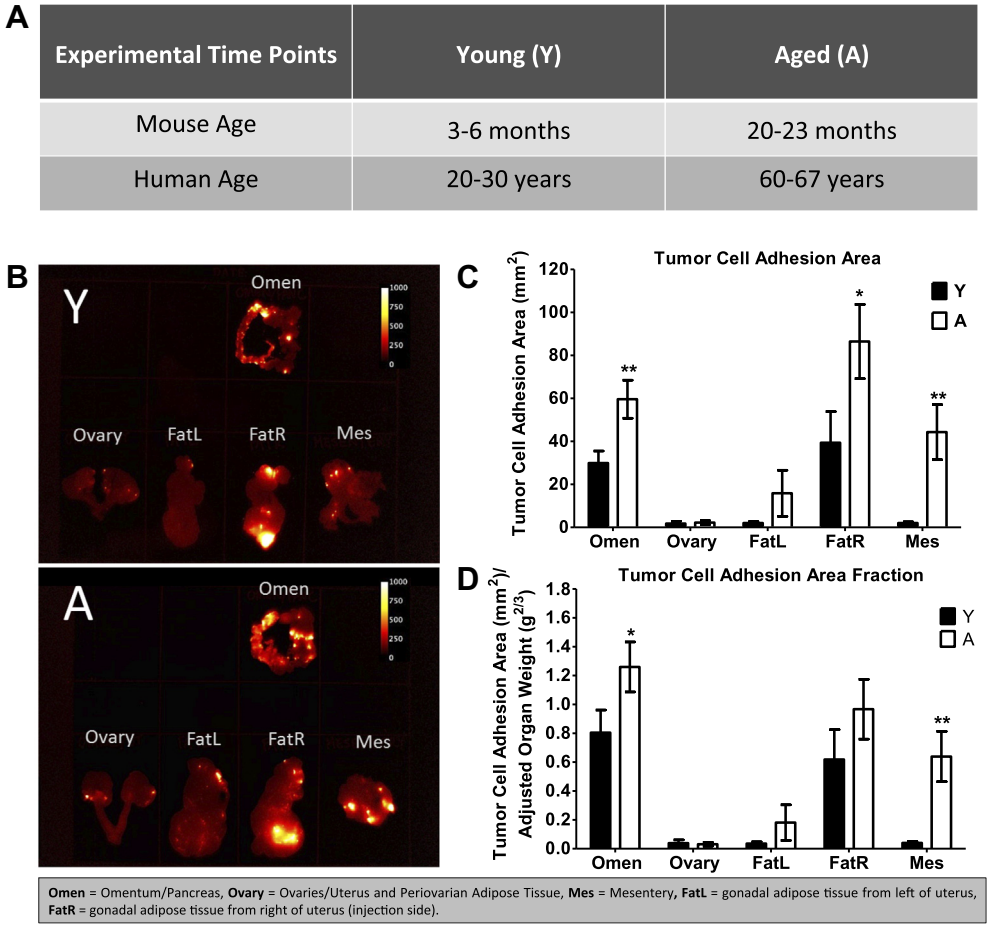

Figure 1. Short-term *in vivo* assay of ID8 cell adhesion to peritoneal adipose tissues. A. Mouse ages and equivalent ages in human years. Mouse ages were chosen based on work by the Harrison Laboratory at Jackson Laboratories [16]. B. Representative tumor cell adhesion images. Young (Y) and Aged (A) mice were injected IP with $4.3x10^6$ ID8 cells tagged with RFP and sacrificed the following day. Major peritoneal adipose depots were dissected and imaged *ex vivo* using the Bruker *In Vivo* Xtreme imaging system. C, D. Quantification of organ-specific tumor cell adhesion. Tumor cell adhesion area (C) was quantified using ImageJ as described in Materials and Methods. For Omen $P = .01$; FatR $P = .05$; Mes $P = .004$. Tumor cell adhesion area fraction (D) was quantified by adjusting for the weight of the organs. N = 10. For Omen $P = .07$; Mes $P = .003$. Double asterisk indicates $P < .05$, single asterisk indicates $P < .1$.

line [18], were tagged with red fluorescent protein (RFP) and maintained as previously described [19]. ID8 cells with a CRISPR/Cas9-generated *Trp53* gene deletion (designated ID8-*Trp53*$^{-/-}$) were generously provided by Dr. McNeish, Glasgow, UK [20] and were RFP-tagged. Cells derived from the oviductal epithelium of FVB/NJ mice and genetically engineered to lack PTEN expression and express oncogenic KRAS [21] (FVB/N-PTEN^{shRNA}/KRAS^{G12V}) were generously provided by Dr. Burdette, Chicago, USA, and were maintained and RFP-tagged as previously described [19,21].

C57Bl/6 young and aged mice (n = 14) were intraperitoneally (IP) injected on the right side of the peritoneal cavity with ID8-RFP cells ($3.7x10^6$) or ID8-*Trp53*$^{-/-}$-RFP cells ($8.7x10^6$) to model dissemination and colonization events of ovarian cancer metastasis. Mice were imaged under isoflurane anesthesia using the Bruker Xtreme *In Vivo* Imaging system and were observed for signs of lethargy or ascites accumulation. Mice were sacrificed by CO_2 anesthesia followed by cervical dislocation. If present, ascites was harvested and volume noted. The ventral skin was pulled away and the peritoneal cavity was exposed with incisions down the center and the sides of the ventral parietal peritoneum. The abdominal organs were scanned *in situ* [19,22], then the organs were removed and imaged *ex vivo*. Note that because tumor cells were injected on the right side, the right and left fat pads were analyzed separately, such that lesions on the left side (designated FatL) represent metastatic seeding whereas the right fat pad (FatR) underwent injection. Images underwent spectral unmixing as previously described [22]. Using ImageJ, tumor burden was analyzed by calculating the tumor area and the intensity of the RFP signal (Raw Integrated Density). In the case of abdominal images, the measurements were corrected using the adjusted body weight of the mouse (weight$^{2/3}$). The adjusted weight of the organs (weight$^{2/3}$) was used to control for animal-to-animal differences in organ size. Statistical analysis used Student's T-test. Studies using FVB/N-PTEN^{shRNA}/KRAS^{G12V} cells were conducted in parallel fashion following IP injection of cells ($3.4x10^6$) into young and aged FVB/NJ mice (n = 14). At ~4.5 weeks, mice were sacrificed and abdominal and organ tumor burden was assessed as described above.

In Vivo Adhesion Assay

To evaluate early events in *in vivo* adhesion [23], young and aged C57Bl/6 mice (n = 10) were injected IP with $4.3x10^6$ ID8-RFP cells, sacrificed the following day, and excised peritoneal fat depots were rinsed with PBS and imaged as described [19,22]. RFP signal was quantified using ImageJ. Statistical analysis was carried out using Student's T-test. The FVB/N-PTEN^{shRNA}/KRAS^{G12V} *in vivo*

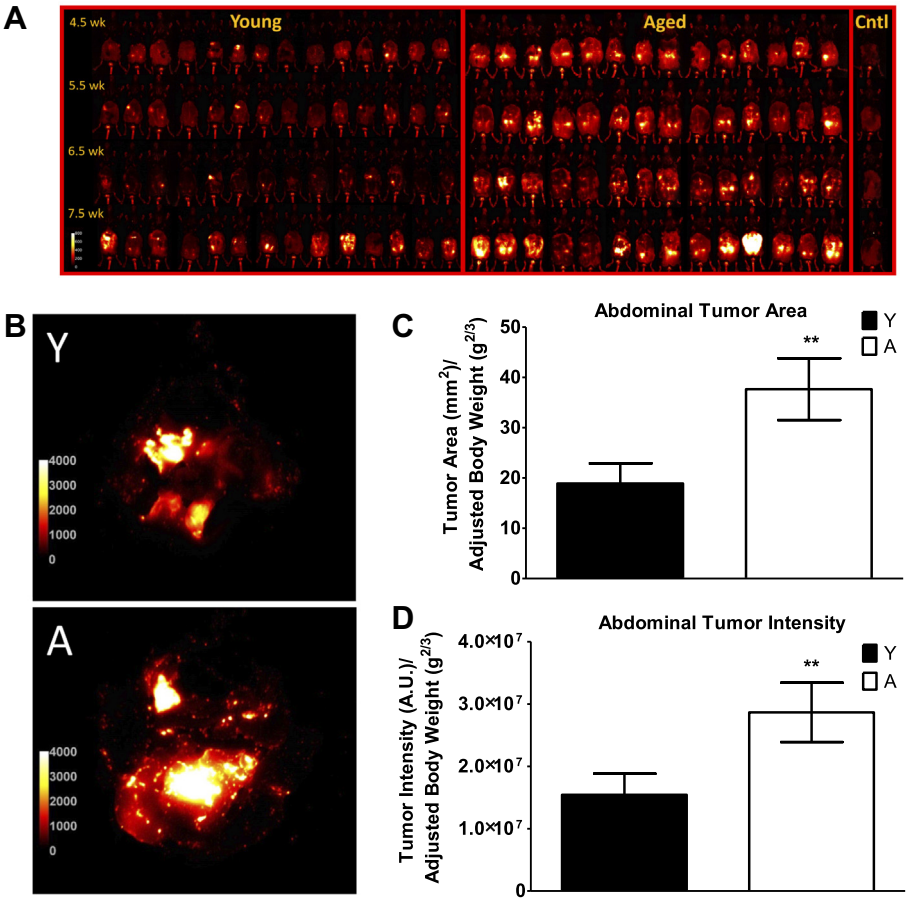

Figure 2. Evaluation of ID8 tumor burden *in situ* of young (Y) and aged (A) C57Bl/6 mice. A. Longitudinal imaging of tumor progression in C57Bl/6 aging cohorts. Mice were injected IP with $3.7x10^6$ ID8 mouse ovarian cancer cells tagged with RFP and were imaged under anesthesia at 4.5, 5.5, 6.5 and 7.5 weeks post injection to monitor tumor progression. Individual mice were followed over the course of 4 weeks. B. Abdominal ID8 tumor burden *in situ*. Mice were sacrificed at 8 weeks post IP injection and each abdominal cavity was exposed and imaged. C, D. Quantification of abdominal tumor burden. Abdominal tumor area (C) and intensity (D), respectively, were quantified by dividing either the tumor area or the tumor intensity by the scale-adjusted body weight of each mouse. N = 14. *P*-values for tumor area and tumor intensity are .02 and .03, respectively. Double asterisk indicates $P < .05$.

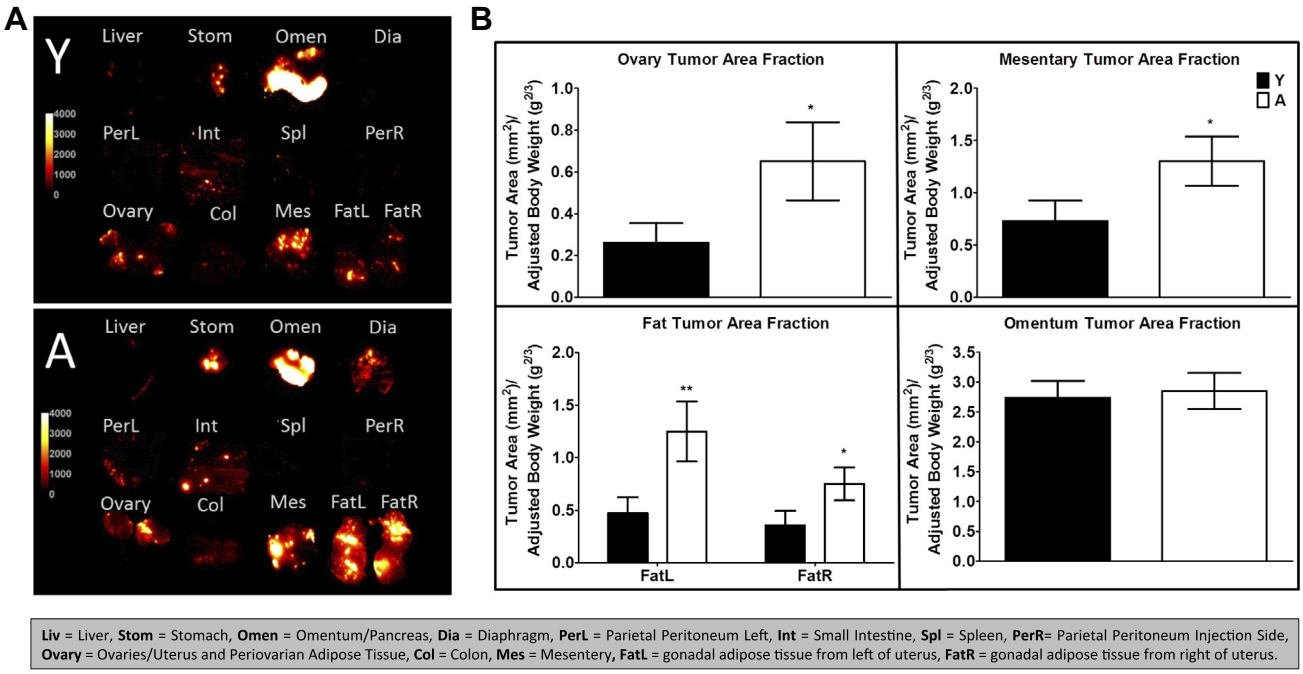

Figure 3. Evaluation of organ-specific ID8 tumor burden of young (Y) and aged (A) C57Bl/6 mice A. Representative tumor burden images. Individual organs were dissected from the mouse peritoneal cavity and imaged *ex vivo*. B. Quantification of organ specific tumor burden. The Organ Area Fraction was quantified by dividing the tumor area by the adjusted organ weight. Organs with significant differences between aged groups are shown, with the omentum as reference. N = 14. For Ovary $P = .07$; Mes $P = .07$; FatL $P = .02$; FatR $P = .07$. Double asterisk indicates $P < .05$, single asterisk indicates $P < .1$.

adhesion study was carried out in a parallel fashion (3.2 x10^6 PTEN^{shRNA}/KRAS^{G12V}-RFP cells were injected into young and aged FVB mice, n = 10 and 9 respectively).

Histological Analysis

Organs were fixed in 10% formalin and paraffin embedded. Tissue sections were stained with H&E according to the specifications of Leica's H&E protocol using SelecTech Define MX-aq, SelecTech Blue Buffer 8, SelecTech Hematoxylin 560 MX, SelecTech Alcoholic Eosin 515. Immunohistochemical analysis of CD45R (protein tyrosine phosphatase receptor type C; lymphocyte common antigen) was performed as described [19] using rat monoclonal anti-CD45R (clone RA3-6B2, 1:800 dilution). Anti-rat IgG and peroxidase detection system reagents (DAB chromogen) were purchased from Abcam, Vector Laboratories, and BioGenex, respectively. Slides were scanned into the eSlide Manager database (version 12.3.2.5030) with the Aperio ScanScope CS (Leica, Biosystems, Inc.). Using Aperio macros, the number of cells stained with DAB chromogen and the total number of cells in tumor sections were quantified. Statistical analysis was carried out using a Student's T-test.

RNA Isolation, RNAseq and Bioinformatics

Gonadal fat was harvested from young and aged mice (n = 4), placed into QIAzol Lysis Reagent (RNeasy Plus Universal Kit), homogenized and RNA was isolated according to the manufacturer's protocol. The Notre Dame Genomics and Bioinformatics Core Facility carried out the RNAseq and bioinformatics analyses. All samples had an RNA Integrity Number (RIN) value greater than or equal to 9. Libraries were constructed using the TruSeq RNA Sample Prep Kit v2 set A and Guide 15,026,495 Rev. F (Illumina, Inc., San Diego, CA). To calculate final library concentration, the quantity and average fragment length was measured using the Agilent Bioanalyzer DNA 7500 Assay (Agilent Technologies, Santa Clara, CA) and Qubit DNA High Sensitivity Assay (Life Technologies Corp.). Libraries were normalized to 20 nM in Buffer EB (Qiagen, Santa Clarita, CA). Equal molar amounts were combined for 100-bp paired-end sequencing on two lanes of HiSeq2500. An average of 46 million raw reads were obtained per sample. Raw sequences were trimmed with Trimmomatic [24] v0.32 and assessed for quality with FastQC [25] v0.11.2. Trimmed sequences were aligned to the Mus_musculus.GRCm38 Ensembl version of the mouse genome, using Mus_musculus.GRCm38.81 annotations, [26] with TopHat2 [27], v2.0.11.Linux_x86_64, using Bowtie 2 [28], v2.2.2. Corresponding alignments were sorted with SAMtools [29], v0.1.19. Read counts were generated with HTSeq-count [30], v0.6.1, and were merged with a python script [31]. Subsequent statistics were completed in R [32], v3.1.0, implementing the EdgeR library [33–35]. Gene names and GO terms were identified using the Ensemble version of BioMart [36]. Metacore Pathway Analysis and Ingenuity Pathway Analysis (IPA) were used to view pathways enriched in differentially expressed genes using a cutoff of $P = .05$.

Quantitative Real-Time PCR

RNA from gonadal adipose tissue was converted to cDNA using a QuantiTect Reverse Transcription Kit (QIAGEN) according to the manufacturer's specifications. qRT-PCR reactions were set up using iTAQ Universal SYBER Green Supermix (BIO-RAD) according to the manufacturer's specifications. A StepOnePlus Real-Time PCR Thermal Cycler System (Applied Biosystems, StepOne Software V2.2.2) was used for qPCR. Primers were custom ordered from Integrated DNA Technologies (Coralville, Iowa). Primers are listed in

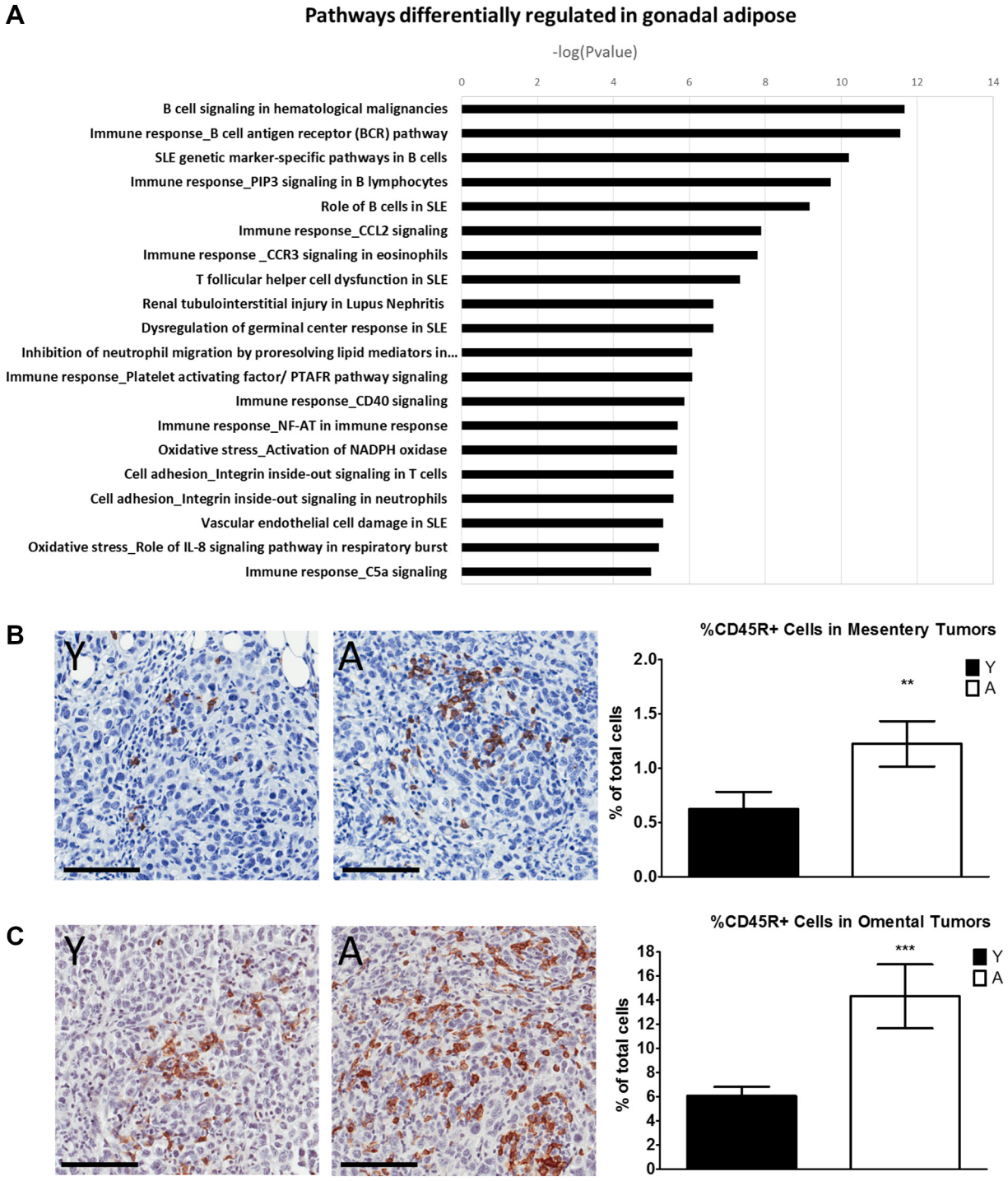

Figure 4. RNASeq analysis of gonadal adipose tissue. A. Representation of differentially regulated pathways in aged gonadal adipose. RNA harvested from gonadal adipose was subjected to RNASeq analysis using the HiSeq2500. Raw sequences were processed and evaluated using Metacore Pathway Analysis. The top 20 pathways from Metacore Pathway Analysis are shown. B, C. IHC analysis of tumor infiltrating lymphocytes in C57Bl/6 ID8 tumor tissue. CD45R+ lymphocytes in (B) mesentery and (C) omental tumor sections were identified by staining with an anti-CD45R antibody (1:800 dilution) followed by a peroxidase-conjugated anti-rat-IgG and peroxidase detection using DAB as described in Methods. Representative images of young and aged tumor tissues are shown. Analysis was carried out with the Aperio Image Analysis Tools package. N = 13, 14 for young (Y), aged (A), respectively. Scale bar = 100 μm. Triple asterisk indicates $P < .01$, double asterisk indicates $P < .05$.

Supplemental Table 1. RSP13 and HPRT were used as endogenous controls to calculate ΔCt values. PCR thermal cycling conditions were as follows: 95 °C for 10 minutes followed by 40 cycles of 95 °C for 15 seconds and 60 °C for 60 seconds. Biological replicates of n = 4 and three technical replicates were utilized for each experiment. The nonparametric Mann–Whitney U Test was selected to determine if ΔCt values of the young and aged samples were significantly different from each other (significance cutoff $P = .05$, analysis carried out in R [32]).

Table 1. qRT-PCR validation panel of B cell related genes upregulated in aged mice. The differential expression of prominent genes in pathways involving B cells in the RNAseq dataset was quantified using qRT-PCR, as described in Materials and Methods. Two normalizer genes, RSP13 and HPRT, were utilized and showed a similar trend N = 4.

Gene	RSP13		HPRT	
	Average Fold Change	*P*-Value	Average Fold Change	*P*-Value
Bank1	8.57	.057	9.18	.029
Blnk	15.78	.057	16.90	.029
Card11	9.59	.029	10.27	.029
CD22	18.25	.029	19.54	.029
CD72	15.45	.029	16.54	.029
CD79a	29.68	.029	31.78	.029
CD79b	26.55	.029	28.43	.029
Ikzf3	11.52	.029	12.34	.029
Pax5	15.78	.029	16.90	.029
Prkcb	6.20	.057	6.64	.029

Results

Epidemiologic data indicate that older women are at greater risk for developing ovarian cancer and receive worse prognoses than younger women [6,8]. As the impact of age on ovarian cancer metastasis has not been evaluated *in vivo*, two syngeneic allograft models of aging and metastasis were selected; the C57Bl/6 ID8 and the FVB/N-PTEN^{shRNA}/KRAS^{G12V} models [18,21]. To explore how age impacts initial adhesion *in vivo,* young and aged C57Bl/6 mice (Figure 1A) were injected IP with ID8-RFP cells ($4.3x10^6$) and sacrificed the following day. Peritoneal adipose tissues, the earliest sites of adhesion in this mouse model of metastasis, were imaged *ex vivo* and analyzed for tumor cell adhesion. Increased tumor cell adhesion was observed to aged adipose tissues relative to the corresponding tissues in young mice (Figure 1B-D).

To investigate if the aged host is more susceptible to metastatic success over an extended period of time during which tumor cells survive and proliferate, young and aged C57Bl/6 mice were injected IP with ID8-RFP cells ($3.7x10^6$) and were imaged longitudinally beginning at 4.5 weeks to monitor tumor progression. Live imaging demonstrated that aged mice developed greater metastatic burden (Figure 2A). Abdominal tumor area and abdominal tumor intensity, parallel methods of analysis, consistently demonstrated aged mice had significantly greater overall tumor burden than their young counterparts (Figure 2B-D). Dissection and analysis *ex vivo* revealed significant age-related differences in tumor burden in the gonadal adipose tissue, with a notable difference also in the mesentery (Figure 3A-B). No difference in metastasis to the omentum was detected, suggesting that over the 8-week incubation, the initial difference in adhesion to the aged omentum was compensated for by matched survival or growth of tumor cells in the young and aged omental fat band. Ascites accumulation was not significantly different. The same trend was observed using virgin young and aged mice, confirming that the parity status of the retired breeders did not confound the results (**Supplemental Fig. 1A-D**).

RNAseq analysis of gonadal adipose tissue was used to explore factors potentially contributing to metastatic success in aged *vs* young animals [37]. Over 1500 genes were significantly differentially expressed ($P < .05$) to varying degrees, ranging from $\log_2$(fold change) -4.86 to 4.35 in the aged animals. Metacore Pathway Analysis and Ingenuity

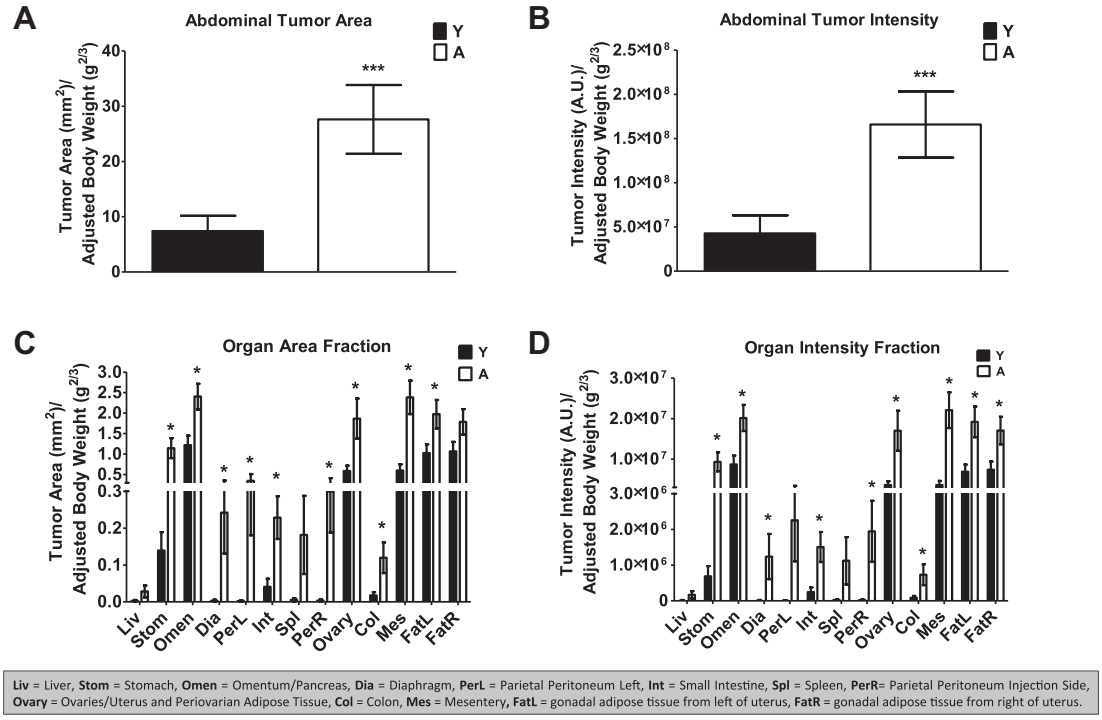

Figure 5. Evaluation of ID8-*Trp53*$^{-/-}$-RFP tumor burden of young (Y) and aged (A) C57Bl/6 mice. A, B. Quantification of abdominal ID8-*Trp53*$^{-/-}$-RFP tumor burden *in situ*. Mice were injected IP with $8.7x10^6$ ID8-*Trp53*$^{-/-}$ mouse ovarian cancer cells tagged with RFP. Mice were sacrificed at 5.5 weeks post IP injection and each abdominal cavity was exposed and imaged. Abdominal tumor area (A) and intensity (B), respectively, were quantified by dividing either the tumor area or the tumor intensity by the scale-adjusted body weight of each mouse. N = 14. *P*-values for tumor area and tumor intensity are 0.005 and 0.006, respectively. C, D. Quantification of organ specific tumor burden. The organ area fraction (C) and intensity (D) were calculated by dividing the tumor area or intensity by the adjusted organ weight. N = 14. Triple asterisk indicates $P < .01$, single asterisk indicates $P < .05$.

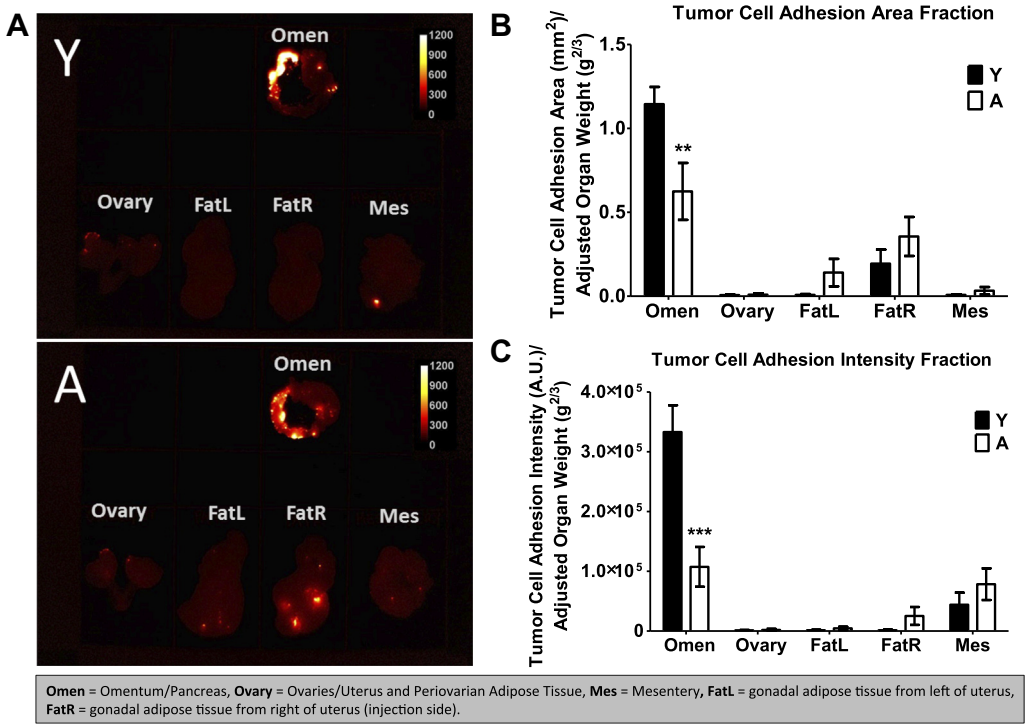

Figure 6. Short-term *in vivo* assay of PTEN^{shRNA}/KRAS^{G12V} cell adhesion to peritoneal adipose tissues. A. Representative tumor cell adhesion images. Young (Y) and Aged (A) mice were injected IP with 3.2x10^6 PTEN^{shRNA}/KRAS^{G12V} RFP-tagged mouse ovarian cancer cells and sacrificed the following day. Major peritoneal adipose depots were rinsed with 1xPBS imaged using the Bruker *In Vivo* Xtreme imaging system *ex vivo*. B, C. Quantification of organ-specific tumor cell adhesion. Tumor Cell Adhesion Area fraction (B) and Intensity Fraction (C) and were quantified using ImageJ as described in Materials and Methods. N = 10, 9 for young and aged, respectively. For Omentum Area Fraction P = .02; Omentum Intensity Fraction P = .001. Triple asterisk indicates P < .01, double asterisk indicates significant P < .05.

Pathway Analysis (IPA) were used to view pathways enriched in differentially expressed genes and these analyses revealed that several upregulated pathways involving lymphocytes, and most notably B cells, were prominent (Figure 4A**; Supplemental Table 2**). As B cells are altered in aging and have prognostic significance in OvCa [38,39], B cell pathway-related genes were chosen for validation by qRT-PCR. Of 11 genes evaluated, 10 were significantly differentially regulated in aged gonadal adipose (Table 1). Concomitant with the increase in B cell markers, CD45R+ lymphocytes were significantly upregulated in tumors from aged mice relative to young mice (Figure 4B-C).

During the course of this study, new sequencing data showed that parental ID8 cells contain wild type *Trp53*, whereas mutations in this gene are highly prevalent in human OvCa [20]. An ID8 derivative was therefore generated using CRISPR/Cas9 to delete *Trp53*, designated ID8-*Trp53*$^{-/-}$ [20]. Using ID8-*Trp53*$^{-/-}$-RFP cells, our results confirm those of Walton and coworkers and show much more rapid IP growth (8 weeks *vs* 5.5 weeks for parental *vs* mutant cells). Furthermore, a significant increase in both overall and organ-specific tumor burden was found in aged mice relative to young mice in this model (Figure 5A-D).

To determine if the age-related effect observed with ID8 cells in C57BL/6 hosts extends to another allograft model, cells derived from the mouse oviductal epithelium were used [21]. These cells mimic fallopian tube-derived OvCa and form aggressive high-grade carcinomas [21]. Young and aged FVB/NJ mice were injected with FVB/N-PTEN^{shRNA}/KRAS^{G12V} cells (3.2x10^6) and sacrificed the following day, followed by imaging of peritoneal adipose tissues *ex vivo*. Surprisingly, analysis revealed the young FVB/NJ mice were more susceptible to tumor cell adhesion at this time point (Figure 6A-C). However when mice were sacrificed and imaged *in situ* and *ex vivo* at 5.5 weeks, aged mice had twice as much abdominal tumor as young mice (Figure 7A-C), with significantly greater tumor burden in multiple tissues including the omentum, mesentery and gonadal adipose tissues Figure 8A-B). Additionally, aged animals accumulated significantly more ascites fluid than did young animals (1.7 +/– 0.3 ml vs 0.4 +/– 0.2 ml, P < .001, respectively).

Discussion

Age is a well-established risk factor for developing OvCa [6]. Furthermore, poorer prognoses are observed in aged individuals, with older women twice as likely to die from OvCa as younger women [8]. A recent epidemiologic study of patients with serous OvCa reported a median overall survival of 37.4 months and 47.6 months for women ages 65 and older and for women under the age of 65, respectively [10]. While a number of factors may be responsible for decreased survival in older women, such as age-related disparities in patient care [11] or coexisting medical conditions, altered cancer aggressiveness in the aged host may also contribute to this phenomenon [8]. Cancer aggressiveness could include properties of the tumor cells themselves and/or the receptivity of the aged host. Studies addressing the impact of the aged peritoneal cavity on OvCa metastasis may offer insights into mechanisms underlying epidemiologic data, particularly the

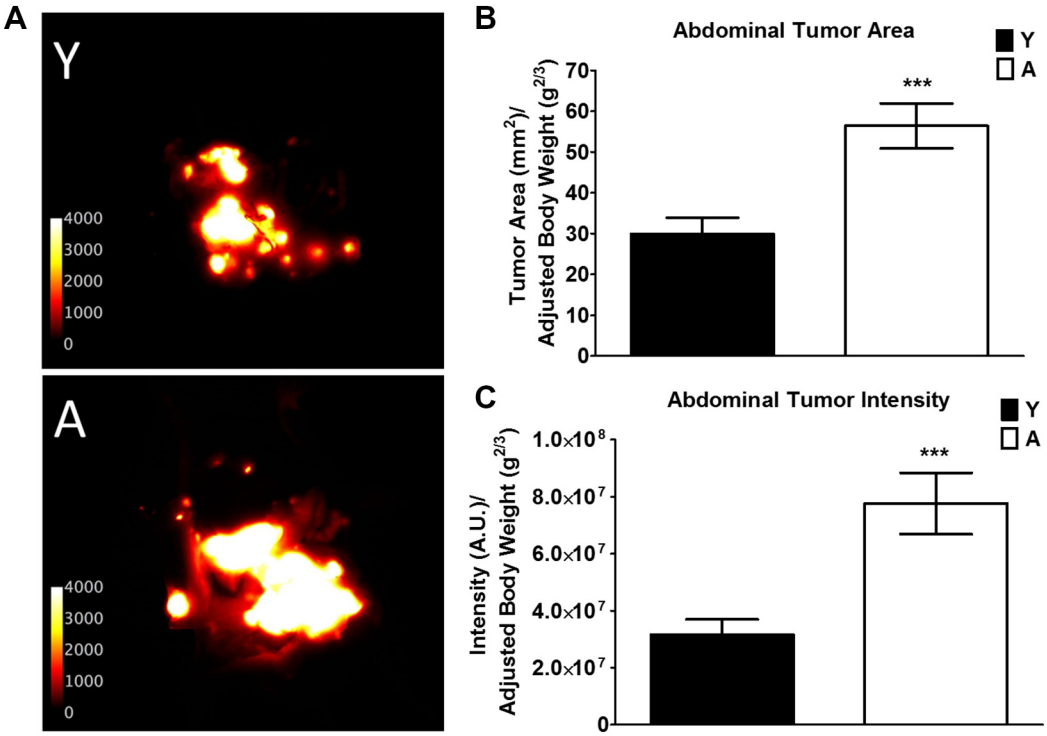

Figure 7. Evaluation of abdominal PTEN^{shRNA}/KRAS^{G12V} tumor burden *in situ* of young (Y) and aged (A) FVB/NJ mice. A. Representative abdominal tumor burden images. Mice were injected IP with 3.4 x 10^6 PTEN^{shRNA}/KRAS^{G12V}-RFP cells. Mice were sacrificed at 4.5 weeks post IP injection and each abdominal cavity was exposed and imaged. B, C. Quantification of abdominal tumor burden. Tumor area (B) and intensity (C), respectively, were quantified by dividing either the tumor area or the tumor intensity by the scale-adjusted body weight of each mouse. N = 14. *P*-values for tumor area and tumor intensity are .0006 and .0007, respectively. Triple asterisk indicates significant $P < .01$.

observed decrease in survival of aged patients, and may expose new therapeutic targets for treatment of aged women with OvCa [6].

It has been proposed that age-related senescence of human omental mesothelial cells (HOMCs) may create a more receptive environment for metastasis as OvCa cells adhere more readily to induced-senescent mesothelial cells *in vitro* [13,40]. Furthermore, HOMCs are in an inflammatory state in the elderly [12]. A single study using a syngeneic murine model of OvCa metastasis reported that age did not significantly alter the immune profile of the murine omental fat band and was ascribed to be a negligible factor in an *in vivo* study addressing the role of parity on OvCa metastasis [14]. This study used middle-aged mice that were 11–12 months old; however there have been no reports regarding the impact of age on OvCa metastasis *in vivo* using truly aged mice (>20 months). Syngeneic murine allograft models with immunocompetent mice provide several advantages in aging and metastasis studies. Such mouse models allow for an intact immune system with which to study the impact of immune cells on cancer progression. Immunocompetent mice also age better than immunocompromised mice without succumbing to other diseases. Working with aged animals can be both expensive and challenging [16], but the current data suggest age is an important factor when investigating OvCa metastasis, warranting further investigation.

Interestingly, various events in metastatic dissemination appear to be differentially effected by age. Short-term *in vivo* adhesion studies with the ID8 C57Bl/6 model revealed that ID8 cells adhered more readily to aged omentum and mesentery compared to young and, at 8 weeks post injection, aged mice had larger overall tumor burden. In contrast, in short-term *in vivo* adhesion studies with the FVB/NJ model, PTEN^{shRNA}/KRAS^{G12V} cells adhered with greater efficacy to the young omentum. Similarly, however, in an extended tumor study, the aged animals also had substantially greater tumor burden. It is interesting to speculate that differential adhesion observed at early time points may reflect distinct profiles of mesothelial senescence in the two murine hosts. Alternatively, differential expression of adhesive ligands and receptors on C57Bl/6 versus FVB/NJ host animals and on tumor cells derived from the ovarian surface epithelium versus oviductal epithelium may also influence early adhesive events *in vivo*. These may include expression of molecules such as P-cadherin, mesothelin/Muc16, CD44/hyaluronic acid, and fibronectin/integrins, Nevertheless, while the two distinct models of age and metastasis varied in the age-related impact on early adhesive events, both consistently demonstrated that the aged host is ultimately more susceptible to IP metastatic colonization.

Our data suggest that age-related changes in the immune cell composition in peritoneal adipose tissue may contribute to metastatic efficiency in aged animals. An unbiased RNAseq approach revealed enrichment of a number of pathways related to B cells in aged C57Bl/6 mouse gonadal adipose tissue and a panel of B cell markers and regulators were validated as significantly upregulated in aged mice relative to young animals. A greater number of TILs were also found in aged ID8 tumors. B cell TILs are associated with prognosis, but reports vary on whether they correspond to positive or negative prognostic significance. Survival in patients with both CD20$^+$ B cell and CD8$^+$ T cell TILs was greater than in patients with CD8$^+$ only TILs [41]. A

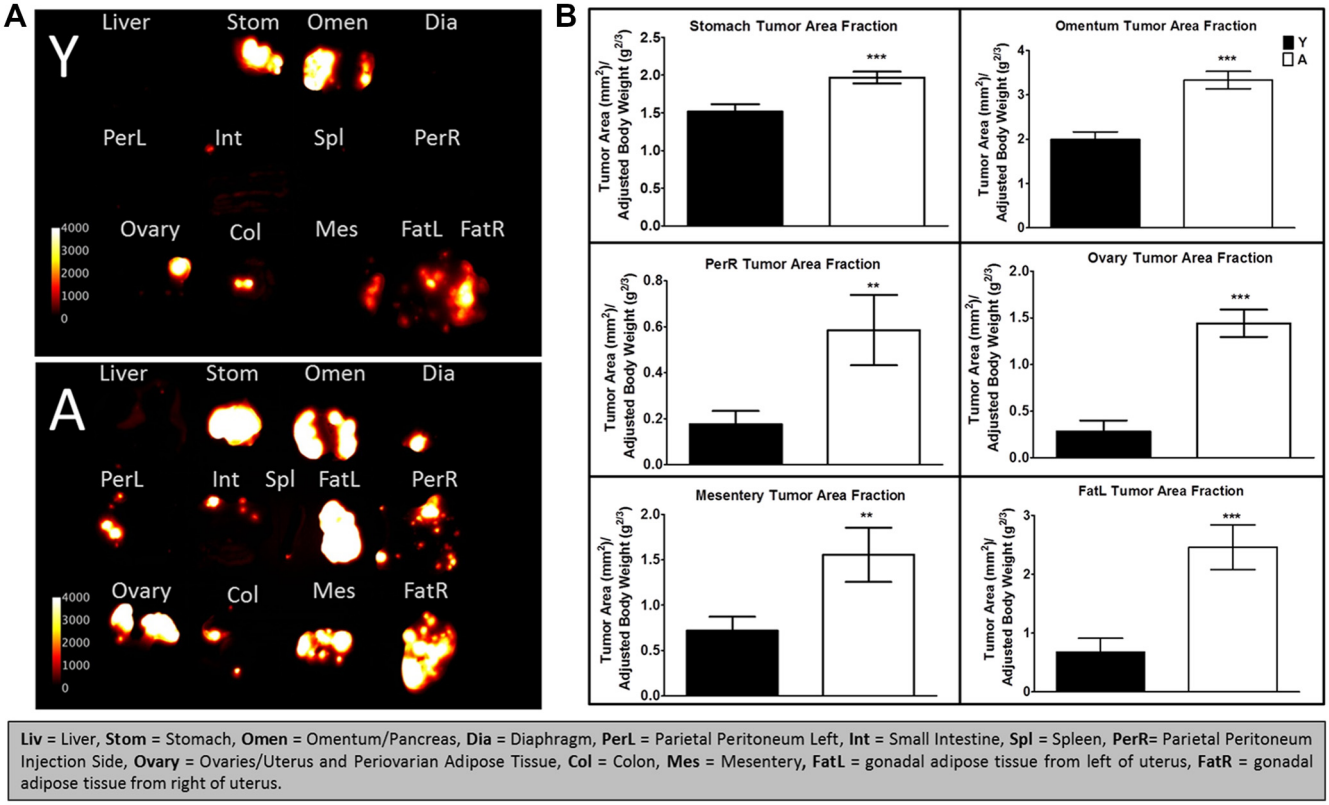

Figure 8. Evaluation of organ-specific PTEN^{shRNA}/KRAS^{G12V} tumor burden of young (Y) and aged (A) FVB/NJ mice. A. Representative tumor burden images. Individual organs were dissected from the mouse peritoneal cavity and imaged *ex vivo*. B. Quantification of organ specific tumor burden. The Organ Area Fraction was quantified by dividing the tumor area by the adjusted organ weight. N = 14. For Organ Stom $P = .001$; Omen $P = .00002$; Ovary $P = .000002$; PerR $P = .019$; Mes $P = .019$; FatL $P = .0005$. Triple asterisk indicates $P < .01$ and double asterisk indicates $P < .05$.

separate study also found that both the presence of CD20$^+$ in the epithelial portion of the tumors and the combination of CD20$^+$ CD8$^+$ were associated with better survival in debulked patients with high-grade serous OvCa [42]. Furthermore, analysis using The Cancer Genome Atlas data revealed that certain B cell receptor expression signatures were predictive of improved survival in immuno-reactive and mesenchymal OvCas [43]. Interestingly, mice with a depleted CD20$^+$ B cell population developed greater tumor burden when injected with ID8 cells [44]. B cells have also been reported as a negative prognostic factor by multiple groups [45,46]. A greater number of CD19$^+$ B cells was correlated with poor survival [46], while more recent data show that high expression of CD19$^+$ B cells in omental ovarian tumors is associated with decreased survival [45]. This same group demonstrated CD19$^+$ B cells promote angiogenesis via STAT3, thereby contributing to disease progression [47]. As CD19 was upregulated in the aged gonadal adipose RNAseq dataset, it is interesting to speculate that the enhanced metastatic tumor burden seen in aged animals in this study may be due to increased angiogenesis.

Among the immunological changes that accompany aging, age-related changes in B cell development and function in humans and in mice have been described [38]. Several groups have recently reported the presence of an age-associated B cell population in aged mice [48,49]. While beyond the scope of this study, further investigation into which subpopulation of B cells are present in the metastatic niche in aged murine models is warranted. Given our findings on the impact of age on metastasis and the literature on age-related changes to B cell populations, future studies which take age into account when investigating the prognostic significance of B cell TILs are needed. Additionally, researchers considering the possibility of modulating B cell response as a therapeutic strategy must consider that age-related differences may impact the contribution of B cells to disease progression.

In summary, here we demonstrate that the aged host is more susceptible to OvCa metastasis in two distinct murine models. Our data suggest a potential contribution of B cells to this age-related disparity in metastatic success. These murine models harbor potential for evaluating immunotherapy interventions in the context of the aged host. Investigating the impact of age on metastasis is timely research, as there is an aging global population and the number of older women diagnosed with OvCa is expected to rise [8]. In addition to continued research in murine models, future research is needed to elucidate the status of B cells in human tumors from patients of varying ages. Such studies are required to predict whether targeting B cells with immunomodulatory therapies is an effective approach in older patients.

Conflict of Interest

There are no known conflicts of interest associated with this publication and there has been no significant financial support for this work that could have influenced its outcome. The manuscript has been read and approved by all named authors and that there are no other persons who satisfied the criteria for authorship but are not

listed. The Corresponding Author (Dr. MS Stack; sstack@nd.edu) is the sole contact for the Editorial process (including Editorial Manager and direct communications with the office). She is responsible for communicating with the other authors about progress, submissions of revisions and final approval of proofs.

Acknowledgements

This work was supported by Grants RO1CA109545 (MSS) from the National Institutes of Health/National Cancer Institute; from the Leo and Anne Albert Charitable Trust (MSS); National Science Foundation Graduate Research Fellowship Program grant DGE-1313583 (EAL); National Institutes of Health/National Cancer Institute KO1 CA218305 (TSH). We thank Freimann Life Sciences Center at the University of Notre Dame, especially Emily Cronberger, for their care of the mice and contributions to the breeding strategy.

Appendix A. Supplementary Data

Supplementary data to this article can be found online at https://doi.org/10.1016/j.neo.2018.03.007.

References

[1] Lengyel E (2010). Ovarian Cancer Development and Metastasis. *Am J Pathol* **177**, 1053–1064 https://doi.org/10.2353/ajpath.2010.100105.

[2] Kurman RJ (2013). Origin and molecular pathogenesis of ovarian high-grade serous carcinoma. *Ann Oncol* **24**(Suppl. 10), x16–21 https://doi.org/10.1093/annonc/mdt463.

[3] Soslow RA (2008). Histologic subtypes of ovarian carcinoma: an overview. *Int J Gynecol Pathol* **27**, 161–174 https://doi.org/10.1097/PGP.0b013e31815ea812.

[4] Pradeep S, Kim SW, Wu Y, Nishimura M, Chaluvally-Raghavan P, and Miyake T, et al (2014). Hematogenous metastasis of ovarian cancer: rethinking mode of spread. *Cancer cell* **26**, 77–91 https://doi.org/10.1016/j.ccr.2014.05.002.

[5] Coffman LG, Burgos-Ojeda D, Wu R, Cho K, Bai S, and Buckanovich RJ (2016). New models of hematogenous ovarian cancer metastasis demonstrate preferential spread to the ovary and a requirement for the ovary for abdominal dissemination. *Transl Res* **175**, 92–102 https://doi.org/10.1016/j.trsl.2016.03.016 [e102].

[6] Howlader N, Noone AM, Krapcho M, Miller D, Bishop K, and Kosary CL, et al (2016). SEER Cancer Statistics Review, 1975–2014, SEER Cancer Statistics Review; 2016.

[7] Thigpen T, Brady MF, Omura GA, Creasman WT, McGuire WP, and Hoskins WJ, et al (1993). Age as a prognostic factor in ovarian carcinoma. The Gynecologic Oncology Group experience. *Cancer* **71**, 606–614.

[8] Tew WP and Lichtman SM (2008). Ovarian cancer in older women. *Semin Oncol* **35**, 582–589 https://doi.org/10.1053/j.seminoncol.2008.08.007.

[9] Hightower RD, Nguyen HN, Averette HE, Hoskins W, Harrison T, and Steren A (1994). National survey of ovarian carcinoma. IV: Patterns of care and related survival for older patients. *Cancer* **73**, 377–383.

[10] Deng F, Xu X, Lv M, Ren B, Wang Y, and Guo W, et al (2017). Age is associated with prognosis in serous ovarian carcinoma. *J Ovarian Res* **10**, 36 https://doi.org/10.1186/s13048-017-0331-6.

[11] Trillsch F, Woelber L, Eulenburg C, Braicu I, Lambrechts S, and Chekerov R, et al (2013). Treatment reality in elderly patients with advanced ovarian cancer: a prospective analysis of the OVCAD consortium. *J Ovarian Res* **6**, 42 https://doi.org/10.1186/1757-2215-6-42.

[12] Nevado J, Vallejo S, El-Assar M, Peiro C, Sanchez-Ferrer CF, and Rodriguez-Manas L (2006). Changes in the human peritoneal mesothelial cells during aging. *Kidney Int* **69**, 313–322 https://doi.org/10.1038/sj.ki.5000082.

[13] Książek K, Mikula-Pietrasik J, Korybalska K, Dworacki G, Jörres A, and Witowski J (2009). Senescent Peritoneal Mesothelial Cells Promote Ovarian Cancer Cell Adhesion : The Role of Oxidative Stress-Induced Fibronectin. *Am J Pathol* **174**, 1230–1240 https://doi.org/10.2353/ajpath.2009.080613.

[14] Cohen CA, Shea AA, Heffron CL, Schmelz EM, and Roberts PC (2013). The parity-associated microenvironmental niche in the omental fat band is refractory to ovarian cancer metastasis. *Cancer Prev Res* **6**, 1182–1193. https://doi.org/10.1158/1940-6207.CAPR-13-0227.

[15] Perez GI, Robles R, Knudson CM, Flaws JA, Korsmeyer SJ, and Tilly JL (1999). Prolongation of ovarian lifespan into advanced chronological age by Bax-deficiency. *Nat Genet* **21**, 200–203 https://doi.org/10.1038/5985.

[16] Flurkey K, Currer JM, and Harrison DE (2007). Chapter 20 - Mouse Models in Aging Research. In: Fox JG, Davisson MT, Quimby FW, Barthold SW, Newcomer CE, Smith AL, editors. The Mouse in Biomedical Research (Second Edition), Academic Press, Burlington; 2007. p. 637–672.

[17] Yuan R, Tsaih SW, Petkova SB, Marin de Evsikova C, Xing S, and Marion MA, et al (2009). Aging in inbred strains of mice: study design and interim report on median lifespans and circulating IGF1 levels. *Aging Cell* **8**, 277–287 https://doi.org/10.1111/j.1474-9726.2009.00478.x.

[18] Roby KF, Taylor CC, Sweetwood JP, Cheng Y, Pace JL, and Tawfik O, et al (2000). Development of a syngeneic mouse model for events related to ovarian cancer. *Carcinogenesis* **21**, 585–591.

[19] Liu Y, Metzinger MN, Lewellen KA, Cripps SN, Carey KD, and Harper EI, et al (2015). Obesity Contributes to Ovarian Cancer Metastatic Success through Increased Lipogenesis, Enhanced Vascularity, and Decreased Infiltration of M1 Macrophages. *Cancer Res.* https://doi.org/10.1158/0008-5472.can-15-0706.

[20] Walton J, Blagih J, Ennis D, Leung E, Dowson S, and Farquharson M, et al (2016). CRISPR/Cas9-Mediated Trp53 and Brca2 Knockout to Generate Improved Murine Models of Ovarian High-Grade Serous Carcinoma. *Cancer Res* **76**, 6118–6129 https://doi.org/10.1158/0008-5472.CAN-16-1272.

[21] Eddie SL, Quartuccio SM, O.h. EMoyle-Heyrman G, Lantvit DD, and Wei JJ, et al (2015). Tumorigenesis and peritoneal colonization from fallopian tube epithelium. *Oncotarget* **6**, 20500–20512 https://doi.org/10.18632/oncotarget.3985.

[22] Lewellen KA, Metzinger MN, Liu Y, and Stack MS (2016). Quantitation of Intraperitoneal Ovarian Cancer Metastasis. *J Vis Exp.* https://doi.org/10.3791/53316.

[23] Nieman KM, Kenny HA, Penicka CV, Ladanyi A, Buell-Gutbrod R, and Zillhardt MR, et al (2011). Adipocytes promote ovarian cancer metastasis and provide energy for rapid tumor growth. *Nat Med* **17**, 1498–1503. http://www.nature.com/nm/journal/v17/n11/abs/nm.2492.html#supplementary-information.

[24] Bolger AM, Lohse M, and Usadel B (2014). Trimmomatic: a flexible trimmer for Illumina sequence data. *Bioinformatics* **30**, 2114–2120 https://doi.org/10.1093/bioinformatics/btu170.

[25] Andrews S (2014). FastQC, Babraham bioinformatics, Babraham institute. http://www.bioinformatics.babraham.ac.uk/projects/fastqc; 2014.

[26] Cunningham F, Amode MR, Barrell D, Beal K, Billis K, and Brent S, et al (2015). Ensembl 2015. *Nucleic Acids Res* **43**, D662–669 https://doi.org/10.1093/bioinformatics/btu170.

[27] Trapnell C, Pachter L, and Salzberg SL (2009). TopHat: discovering splice junctions with RNA-Seq. *Bioinformatics* **25**, 1105–1111 https://doi.org/10.1093/bioinformatics/btp120.

[28] Langmead B and Salzberg SL (2012). Fast gapped-read alignment with Bowtie 2. *Nat Methods* **9**, 357–359 https://doi.org/10.1038/nmeth.1923.

[29] Li H, Handsaker B, Wysoker A, Fennell T, Ruan J, and Homer N, et al (2009). The Sequence Alignment/Map format and SAMtools. *Bioinformatics* **25**, 2078–2079 https://doi.org/10.1093/bioinformatics/btp352.

[30] Anders S, Pyl PT, and Huber W (2015). HTSeq–a Python framework to work with high-throughput sequencing data. *Bioinformatics* **31**, 166–169 https://doi.org/10.1093/bioinformatics/btu638.

[31] Wheeler D (2013). How to use DESeq to analyse RNAseq data, David Wheeler Lab. https://dwheelerau.com/2013/2004/2015/how-to-use-deseq-to-analyse-rnaseq-data/; 2013.

[32] R-Core-Team (2014). A language and environment for statistical computing. Vienna, Austria: R Foundation for Statistical Computing; 2014 http://www.R-project.org/.

[33] McCarthy DJ, Chen Y, and Smyth GK (2012). Differential expression analysis of multifactor RNA-Seq experiments with respect to biological variation. *Nucleic Acids Res* **40**, 4288–4297 https://doi.org/10.1093/nar/gks042.

[34] Robinson MD, McCarthy DJ, and Smyth GK (2010). edgeR: a Bioconductor package for differential expression analysis of digital gene expression data. *Bioinformatics* **26**, 139–140 https://doi.org/10.1093/bioinformatics/btp616.

[35] Robinson MD and Smyth GK (2007). Moderated statistical tests for assessing differences in tag abundance. *Bioinformatics* **23**, 2881–2887 https://doi.org/10.1093/bioinformatics/btm453.

[36] Kinsella RJ, Kahari A, Haider S, Zamora J, Proctor G, and Spudich G, et al (2011). Ensembl BioMarts: a hub for data retrieval across taxonomic space. *Database (Oxford)* **2011**, bar030 https://doi.org/10.1093/database/bar030.

[37] Loughran EA, Phan RC, Leonard AK, Tarwater L, Asem M, and Liu Y, et al (2017). Multiparity activates interferon pathways in peritoneal adipose tissue and decreases susceptibility to ovarian cancer metastasis in a murine allograft model. *Cancer Lett.* https://doi.org/10.1016/j.canlet.2017.09.028.

[38] Kogut I, Scholz JL, Cancro MP, and Cambier JC (2012). B cell maintenance and function in aging. *Semin Immunol* **24**, 342–349 https://doi.org/10.1016/j.smim.2012.04.004.

[39] Santoiemma PP and Powell Jr DJ (2015). Tumor infiltrating lymphocytes in ovarian cancer. *Cancer Biol Ther* **16**, 807–820 https://doi.org/10.1080/15384047.2015.1040960.

[40] Ksiazek K (2013). Mesothelial cell: a multifaceted model of aging. *Ageing Res Rev* **12**, 595–604 https://doi.org/10.1016/j.arr.2013.01.008.

[41] Nielsen JS, Sahota RA, Milne K, Kost SE, Nesslinger NJ, and Watson PH, et al (2012). CD20+ tumor-infiltrating lymphocytes have an atypical CD27- memory phenotype and together with CD8+ T cells promote favorable prognosis in ovarian cancer. *Clin Cancer Res* **18**, 3281–3292 https://doi.org/10.1158/1078-0432.CCR-12-0234.

[42] Milne K, Kobel M, Kalloger SE, Barnes RO, Gao D, and Gilks CB, et al (2009). Systematic analysis of immune infiltrates in high-grade serous ovarian cancer reveals CD20, FoxP3 and TIA-1 as positive prognostic factors. *PLoS One* **4**, e6412 https://doi.org/10.1371/journal.pone.0006412.

[43] Iglesia MD, Vincent BG, Parker JS, Hoadley KA, Carey LA, and Perou CM, et al (2014). Prognostic B-cell signatures using mRNA-seq in patients with subtype-specific breast and ovarian cancer. *Clin Cancer Res* **20**, 3818–3829 https://doi.org/10.1158/1078-0432.CCR-13-3368.

[44] Montfort A, Pearce O, Maniati E, Vincent BG, Bixby L, and Bohm S, et al (2017). A Strong B-cell Response Is Part of the Immune Landscape in Human High-Grade Serous Ovarian Metastases. *Clin Cancer Res* **23**, 250–262 https://doi.org/10.1158/1078-0432.ccr-16-0081.

[45] Yang C, Lee H, Jove V, Deng J, Zhang W, and Liu X, et al (2013). Prognostic significance of B-cells and pSTAT3 in patients with ovarian cancer. *PLoS One* **8**, e54029 https://doi.org/10.1371/journal.pone.0054029.

[46] Dong HP, Elstrand MB, Holth A, Silins I, Berner A, and Trope CG, et al (2006). NK- and B-cell infiltration correlates with worse outcome in metastatic ovarian carcinoma. *Am J Clin Pathol* **125**, 451–458.

[47] Yang C, Lee H, Pal S, Jove V, Deng J, and Zhang W, et al (2013). B cells promote tumor progression via STAT3 regulated-angiogenesis. *PLoS One* **8**, e64159 https://doi.org/10.1371/journal.pone.0064159.

[48] Hao Y, O'Neill P, Naradikian MS, Scholz JL, and Cancro MP (2011). A B-cell subset uniquely responsive to innate stimuli accumulates in aged mice. *Blood* **118**, 1294–1304 https://doi.org/10.1182/blood-2011-01-330530.

[49] Rubtsov AV, Rubtsova K, Fischer A, Meehan RT, Gillis JZ, and Kappler JW, et al (2011). Toll-like receptor 7 (TLR7)-driven accumulation of a novel CD11c (+) B-cell population is important for the development of autoimmunity. *Blood* **118**, 1305–1315 https://doi.org/10.1182/blood-2011-01-331462.